Available online at www.sciencedirect.com
ScienceDirect
Trans. Nonferrous Met. Soc. China 28(2018) 1755−1762
Transactions of Nonferrous Metals Society of China
www.tnmsc.cn

Effect of addition of Si on microstructure, mechanical properties, bio-corrosion and cytotoxicity of Mg−6Al−1Zn alloy

M. AMIRNEJAD, M. RAJABI, A. MOTAVALLI

Department of Materials Science and Engineering, Faculty of Mechanical Engineering, Babol Noshirvani University of Technology, P. O. Box 47148-71167, Shariati Street, Babol, Iran

Received 12 September 2017; accepted 3 February 2018

Abstract: The Mg−6Al−4Zn alloy was fabricated by mechanical alloying (MA) and hot pressing to serve as biodegradable metal implant. The influence of addition of 1% Si (mass fraction) on the microstructure, mechanical properties and bio-corrosion behavior of Mg−6Al−1Zn alloy was studied using X-ray diffractometry, transmission electron microscopy, compression test, as well as immersion, electrochemical test and MTT assay. The results showed that the addition of 1% Si to Mg−6Al−1Zn alloy led to the formation of fine Mg_2Si phase with polygonal shape, and increased compressive strength, elongation and improved corrosion resistance. Furthermore, the cell viability of Saos-2 cells has been improved by addition of 1% Si to Mg−6Al−1Zn alloy. According to the results, the magnesium ions released in the methylthiazol tetrazolium (MTT) test have not shown any cell toxicity. All these indicated that the addition of 1% Si improved the properties of Mg−6Al−4Zn alloy for using as a biodegradable implant.
Key words: Mg-based alloy; mechanical alloying; mechanical properties; corrosion rate; cell viability

1 Introduction

There is a great deal of interest in using degradable alloys in a number of critical medical applications after many years of planning strategies to decrease the corrosion of metallic biomaterials [1]. Mg-based alloys possess a combination of desirable properties as metallic implants in orthopaedic application including low density, good elastic modulus and compressive yield strength closer to those of natural bones, as well as their high specific strength ratio [2−4]. However, the main limitation on applying magnesium alloy as an orthopaedic biomaterial is that degradation occurs before the formation of stable tissue around the implant [5]. A suitable elemental composition can improve the corrosion resistance and mechanical properties of Mg-based materials [6,7]. To fulfil the requirements of a degradable implant, the elements used in alloys must be selected considering the possible systemic effects resulted from their application in the physiological system.

Mg-based alloys containing 2%−10% Al (mass fraction) indicate moderate corrosion resistance and improved mechanical properties due to the protection of aluminum oxide film and the strengthening of the Al element [7−11]. Adding Zn element to Mg-based alloys enhances both the mechanical properties and the corrosion resistance [12]. Zn as an alloying element has been found to be next to Al in strengthening effectiveness in magnesium alloys [11,12]. YIN et al [13] have shown that adding Zn element to Mg-based alloys improved both the tensile strength and the corrosion resistance successfully. Moreover, Zn helps to defeat the negative corrosive effect of iron and nickel impurities, and improves the corrosion properties [13−15]. Zn is recognized as a highly essential element for human body. In zinc inadequacy, most of the physiological functions are strongly interrupted [15]. Recently, Si has been considered as an essential mineral in the human body [11,16]. It plays a significant role in both aiding the healing process and building the immune system [17]. Moreover, it is an important factor for the growth and envelopment of bone and connective tissue [18].

The intermetallic compound Mg_2Si is a stable phase with low density, high elastic modules and high specific strength [19]. The production of Mg_2Si by conventional methods tends to result in heterogeneous microstructure

Corresponding author: M. RAJABI; Tel: +98-11-32334205; Fax: +98-11-32312268; E-mail: m.rajabi@nit.ac.ir
DOI: 10.1016/S1003-6326(18)64819-8

with undesirable coarse grains [18−20]. Solid-state synthesis of Mg_2Si by mechanical alloying of elemental powders has also been investigated [21,22]. However, it is usually difficult to synthesize Mg_2Si by direct mechanical milling due to the stable oxide films formed on the Mg particles [23]. It has been reported that the morphology modification of Mg_2Si phase from coarse Chinese-script shape to small polygonal shape can efficiently improve the mechanical properties [17,18]. SRINIVASAN et al [17] has reported that fine and distributed Mg_2Si phase with polygonal shape has effectively reduced the corrosion rate compared to the coarse Chinese-script Mg_2Si in AZ91 magnesium alloy.

The present study focused on the effect of Si addition on the microstructure, mechanical properties, bio-corrosion and cytotoxicity of nanocrystalline Mg−6Al−1Zn alloy prepared by mechanical alloying and hot pressing.

2 Experimental

Elemental powders of Mg (purity >97%, Merck), Al (purity >98%, Merck), Zn (purity >99.9%, Merck) and Si (purity >98%, Sigma) were used as starting materials. The powder mixture blended with nominal composition of Mg−6Al−1Zn and Mg−6Al−1Zn−1Si (mass fraction, %) has mechanically been alloyed in a Retsch PM100 planetary ball mill at room temperature for 50 h. The ball-to-powder mass ratio was about 20:1 and rotation speed was adjusted to be 250 r/min. The planetary ball mill was periodically stopped every 25 min for 5 min. Stearic acid was used as the process control agent, and the amount was 3% (mass fraction). Weighing, filling and handling of the powder were performed in a glove box under argon atmosphere.

Consolidation of the milled powders was performed in a steel die (internal diameter of 10 mm) at 350 °C under applied pressure of 300 MPa for 60 min in a high purity argon atmosphere. The phase constituents of the as-milled powders and the consolidated specimens were analyzed by X-ray diffraction (XRD, X′Pert Pro MPD, PANalytical) with Cu K_α radiation. The grain size of the obtained powder has been estimated from the broadening of XRD peaks using Williamson–Hall method [24]. The microstructure of the consolidated samples was investigated by transmission electron microscopy (TEM, Philips CM200 FEG) operated at 200 kV. To characterize the intermetallic phases, in TEM analysis, bright field image technique, selected area diffraction (SAD) and EDS methods have been used. The mechanical properties of the compacts have been examined by compression test. A servo-control machine (Gotech, AI−7000L, China) at a strain rate of 1.66×10^{-3} s^{-1} was utilized for the compression test. The test temperature was 25 °C. Vickers microhardness test of the compacts was conducted using a hardness tester (Instron Wolpert, Germany) at the indentation load of 1 kg and 30 s.

The electrochemical measurement of samples has been performed by autolab potentiostat/galvanostat (model 302N, Netherlands) connected to a PC (Software NOVA 1.6) and equipped with electrochemical impedance spectroscopy module. The test was carried out in aerated Ringer physiological solution (NaCl 9 g/L, $CaCl_2$ 0.24 g/L, KCl 0.42 g/L and $NaHCO_3$ 0.2 g/L) at room temperature. Prior to the test, the samples were kept in the solution for 1 h. The electrochemical measurements were performed with a standard three-electrode cell consisting of a saturated calomel reference electrode (SCE), a platinum counter electrode, and the samples as working electrode.

For the evaluation of corrosion rates, the immersion test was carried out according to ASTM-G31-72 [25] in Ringer physiological solution. Samples (10 mm (diameter) × 2 mm (height)) were immersed in 50 mL of solution at 37 °C. The pH value of solution was recorded after each incubation period. The samples were taken out from Ringer solution. The corroded samples were cleaned with distilled water and dried at room temperature. These samples were immersed in 180 g/L chromate acid for 5 min to remove the corrosion products adhered to the samples. Subsequently, they were rinsed with distilled water and dried again at room temperature. The dried samples were weighed and the corrosion rate was calculated as follows [26]:

$$C_R=m/(At) \quad (1)$$

where C_R is the corrosion rate (mg/(cm^2·h)), m is the mass loss (mg), A is the original surface area revealing to the test solution (cm^2) and t is the exposure time (h).

Methylthiazol tetrazolium (MTT) test was used to determine the cell toxicity. Saos-2 cells were used to evaluate the cytotoxicity of samples. A 100 mg portion of each sterilized sample was submerged in 400 μL of complete medium (Dulbecco's modified Eagle's medium−DMEM) and incubated at 37 °C for 72 h. The obtained extracts were diluted with the same volume of the complete medium to be used as an exposure medium. The Saos-2 cells at the 5th passage were seeded in 96 well plates at a density of 1×10^4 cell/well, and 200 μL of the corresponding exposure medium was added to each well. The complete medium was used as a control group. The cytotoxicity and effects on proliferation of the biomaterial extracts were assessed by MTT (Sigma, UK) assay. The Saos-2 cells seeded in 96 well plates were exposed to the sample extracts for 48 h. The medium was then replaced by 50 μL of 0.5% MTT solution in phosphate buffered saline (PBS) and the cells were incubated at 37 °C for another 4 h. Thereafter, the

blue precipitated formazan dye was dissolved in 150 μL acidic isopropanol (0.4 mol/L HCl) by shaking. The optical density of the wells was measured at 570 nm in 20−30 min using a microtiter spectrophotometer (Rayto Elisa Reader, China). The culture plate was shaken for 2 min in order to obtain uniform dyeing and 630 nm was used as a reference wave length. The average optical density of control group (complete medium) was considered as 100%. Accordingly, the average optical densities of other samples were calculated and presented as a percentage of the control group optical density. The one-way ANOVA statistical analysis was used to evaluate the statistical significance of the MTT results. Turkey's HSD multiple comparison testing was used to determine the significance of the deviations in each sample. In all cases, the results have been considered to be statistically different at $P<0.05$ ($n=3$).

The inductively coupled plasma (ICP-OES, Varian vista-pro) was employed to measure the concentrations of magnesium ions which were dissolved from the sample plates in all extracts.

3 Results and discussion

3.1 Microstructure and mechanical properties

Figure 1 shows the XRD patterns of the powder mixtures before and after milling for 50 h. As can be seen, milling the powders causes the diffraction peaks to become broader, but the intensities decrease. The peak broadening can be attributed to the refined grains and the stored energy of cold-deformed structure [26,27]. In both systems, the diffraction peaks of $MgAl_2O_4$ phase are detected, showing the oxidation of magnesium during the process. It is considerable that Al peaks have existed in both mechanical alloyed samples, indicating the incomplete solubility of Al in Mg matrix. At equilibrium state, the intermetallic phase of Mg_2Si has been formed by adding Si to Mg [16,20]. The results of the present study indicate that Mg_2Si intermetallic compound has not been formed in the as-milled Mg−Al−Zn−Si system, which is similar to the reported results of the previous studies [21,22]. This can be attributed to the formation of stable oxide film on the Mg particles, inhibiting the diffusion of Si and Mg atoms. In general, direct synthesis of Mg_2Si by mechanical milling at temperatures much lower than the melting point of magnesium would be difficult, as stated by WANG and QIN [22] for the formation of nanocrystalline Mg_2Si through solid-state reaction.

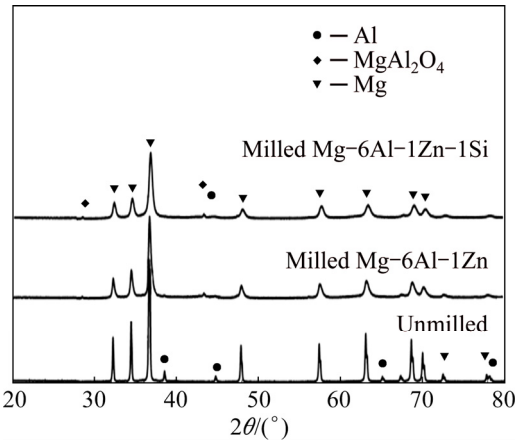

Fig. 1 XRD patterns of unmilled, milled Mg−6Al−1Zn and milled Mg−6Al−1Zn−1Si

Figure 2 shows the XRD patterns of the hot-pressed compacts. The considerable point is that in both systems, diffraction peaks of $Mg_{17}Al_{12}$ can be seen. In Mg−6Al−1Zn−1Si system, the peaks corresponding to Mg_2Si phase have been detected. To further characterize the microstructures, TEM has been employed.

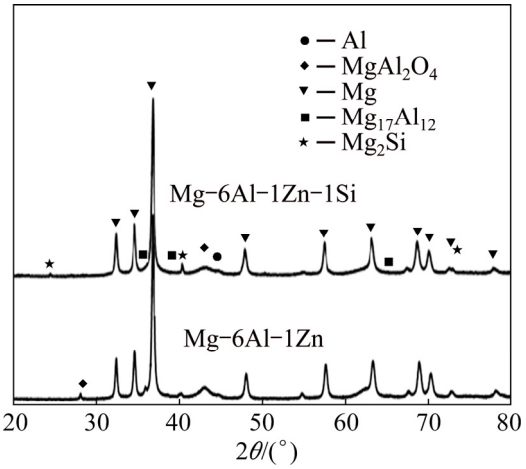

Fig. 2 XRD patterns of hot-pressed compacts

Figure 3 shows a bright field TEM image, diffraction pattern and EDS spectrum of the Mg−6Al−1Zn−1Si compact. Ultrafine Mg_2Si particles with an average diameter of 50 nm have been observed. It has been shown that the reaction of Mg to Si and formation of Mg_2Si take place at very high temperatures due to oxide films (MgO and/or SiO_2) covering the particles [22]. However, some processes like mechanical alloying can refine microstructures and represent defects, facilitating the subsequent solid-state reaction of Mg to Si. SUN et al [19] has concluded that at 545 °C, the synthesis of in-situ Mg_2Si compound from Mg and Si elemental powders can be formed. According to WANG and QIN [22], after milling for 60 h, the formation temperature of Mg_2Si has decreased from ~460 to ~180 °C in Mg−37%Si system. When the oxide films have been cracked as a result of milling, the fresh surfaces have caused the Mg contact directly with Si. Consequently, Mg has started to react with Si at a lower temperature for the milled powder.

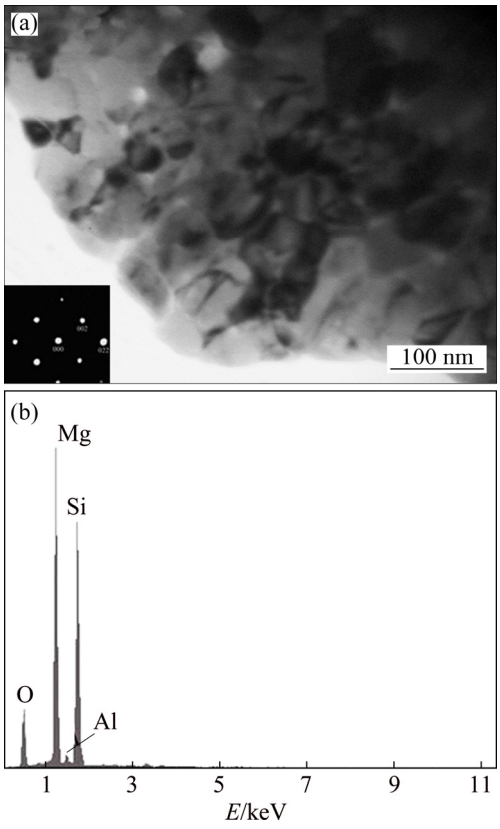

Fig. 3 TEM bright field image (inset showing SAD pattern) (a) and EDS spectrum (b) of intermetallic phase for 50 h-milled sample hot-pressed at 350 °C for 1 h

The mechanical properties of the consolidated powders are reported in Table 1. About grain size determination by Williamson−Hall method, it should be noted that this method is based on the broadening of the diffraction lines due to the strain and crystallite size. The Williamson–Hall equation is expressed as follows:

$$B_S\cos\theta=K\lambda/D+2\varepsilon\sin\theta \quad (2)$$

where B_S is the full width at half-maximum of the mechanically alloyed powders peaks, K is the Sherrer constant, D is the crystallite size, ε is the internal strain, λ is the wavelength of X-ray and θ is the Bragg angle. B_S was calculated as follows:

$$B_S^2 = B_m^2 - B_c^2 \quad (3)$$

where B_m is the evaluated width and B_c is the width at half-maximum of the Mg powder peaks used for calibration.

Two important observations which have been observed during the consolidation process are α-Mg grain coarsening and precipitation of the Mg_2Si intermetallic compound (Fig. 3 and Table 1). By adding Si, the compressive strength has been increased from 290 to 313 MPa. Moreover, the elastic modulus and ductility by adding 1% Si have the same trend, increasing from 53 GPa and 5.5% to 57 GPa and 5.7%, respectively. The results of the hardness measurements show that adding Si leads to an increase in the hardness of hot-pressed compacts (see Table 1) and can be attributed to the finer grain size [28]. It is reported that the dispersion of second-phase reduces the rate of grain growth because the driving pressure for the grain growth is compensated by the pinning force from the particles. Grain growth inhibition associated with dispersed second-phase particles has been reported in a wide variety of nonferrous metals [29]. According to LUCAK and TROJANOVA [30], the increase in ductility of sample with grain refinement is due to the activity of glide in a non-basal slip system and the strain hardening rate influenced by grain size. Here, a higher strength value is obtained due to the fine grain size and formation of Mg_2Si intermetallic phase.

Table 1 Compressive properties and grain sizes of as-milled powders and hot-pressed compacts (d_p is as-milled grain size, d_s is hot-pressed grain size, E is elastic modulus, and σ_c is compressive strength)

Sample	d_p/ nm	d_s/ nm	E/ GPa	σ_c/ MPa	Ductility/ %	Hardness (HV)
Mg−6Al−1Zn	47	71	53	290	5.5	120
Mg−6Al−1Zn−1Si	41	63	57	313	5.7	137

3.2 Bio-corrosion behavior evaluation

3.2.1 Electrochemical test

The corrosion behavior of the hot-pressed compacts has been studied by potentiodynamic polarization. The potentiodynamic curves of compacts are shown in Fig. 4. The polarization data obtained for compacts including corrosion potential (φ_{corr}), corrosion rate (v_{corr}) and corrosion current density (J_{corr}) are summarized in Table 2. It can be seen from Fig. 4 and Table 2 that, the corrosion potential of the Mg−6Al−1Zn−1Si is ~210 mV nobler as compared to that of Mg−6Al−1Zn alloy, showing a considerably less susceptibility of the Mg−6Al−1Zn−1Si alloy to corrosion. The addition of 1% Si has improved the corrosion resistance of Mg−6Al−1Zn alloy due to the formation of refined polygonal-shaped Mg_2Si phase. The Mg_2Si phase as a second phase has a dual effect on corrosion behavior of Mg−Al−Zn alloy. At low volume fraction of Mg_2Si phase (Chinese script type), the corrosion resistance will be decreased due to the cathodic effect of intermetallic phase compared to Mg matrix; while when the volume fraction of Mg_2Si phase is high, the continuous network of polygonal type Mg_2Si acts as a barrier to corrosion due to the stabilized oxide/hydroxide protective layer on magnesium [31]. It has been reported that the morphology and distribution of second phases have

played an important role in the corrosion properties of magnesium alloys [16,22]. For example, SRINIVASAN et al [17] have reported that the morphology and distribution of Mg_2Si intermetallic phase have influenced the corrosion behavior of AZ91magnesium alloys greatly. BEN-HAMU et al [32] have found that adding 0.5% Si (mass fraction) to Mg−6Zn−0.5Mn alloy reduced its corrosion resistance significantly, though the corrosion resistance has been improved when Si content has reached 1% and 2% due to the refinement of Mg_2Si phase. The existence of both Zn and Si can also refine the morphology of Mg_2Si phases effectively and may introduce a small amount of Mg−Zn phases which have also influenced the corrosion properties positively [12].

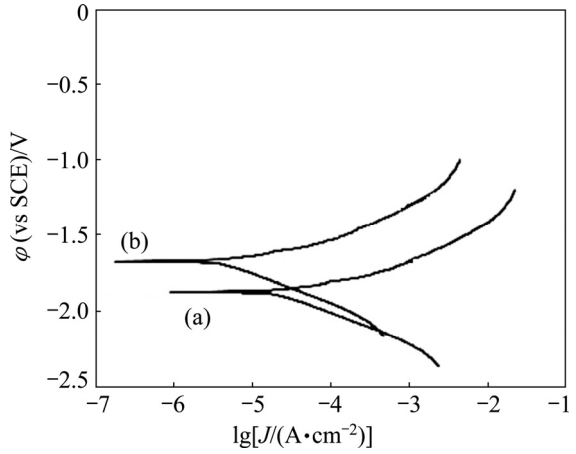

Fig. 4 Electrochemical polarization curves of Mg−6Al−1Zn (a) and Mg−6Al−1Zn−1Si (b) alloys in Ringer solution

Table 2 Electrochemical corrosion data in Ringer solution at 37 °C

Sample	v_{corr}/(mm·year^{-1})	J_{corr}/(μA·cm^{-2})	φ_{corr}/V
Mg−6Al−1Zn	2.44	107.12	−1.86
Mg−6Al−1Zn−1Si	1.94	86.06	−1.65

3.2.2 Immersion test

Figure 5 shows corrosion rates of the immersed compacts in the Ringer physiological solution as a function of the immersion time. In both systems, the corrosion rate decreased with increasing time of immersion. The total corrosion rate of Mg−6Al−1Zn alloy has been measured to be 4.1 mg/(cm^2·h) after 24 h of immersion; however, for Mg−6Al−1Zn−1Si system, the total corrosion rate after 24 h has been measured to be 3.4 mg/(cm^2·h). These results are very much in line with polarization test. As stated in Section 3.2.1, this retardation of the corrosion of the Si-containing system may be explained by the formation of refined Mg_2Si phase that acts as a barrier to corrosion due to the stabilized oxide/hydroxide protective layer on magnesium.

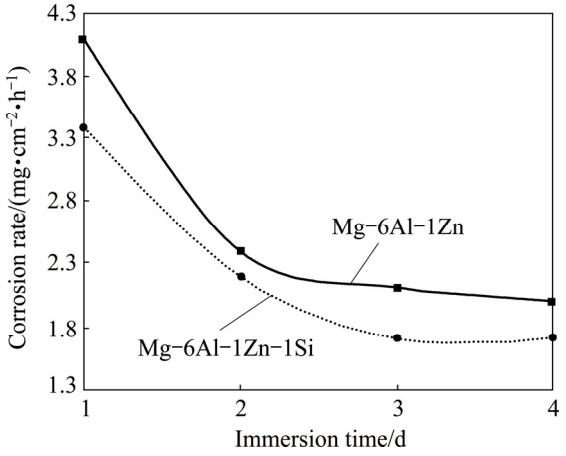

Fig. 5 Corrosion rate of immersed Mg−6Al−1Zn and Mg−6Al−1Zn−1Si alloys in Ringer solution as function of immersion time

It can be seen from Fig. 6 that the corrosion product after immersion contains $Mg(OH)_2$ and MgO. Magnesium is a very active metallic element. When magnesium alloy is immersed into Ringer solution, it will dissolve in solution and reacts with water. As a result, $Mg(OH)_2$ will be formed on the surface of magnesium. The dissolution of magnesium in aqueous solution includes the following reactions [33,34]:

$$Mg \rightarrow Mg^{2+}+2e \quad (4)$$

$$2H_2O+2e \rightarrow H_2+2OH^- \quad (5)$$

$$Mg^{2+}+2OH^- \rightarrow Mg(OH)_2 \quad (6)$$

It is indicated that high corrosion rate at a pH value above 9 is essential to formation of $Mg(OH)_2$ [30]. Before 24 h exposure, magnesium will dissolve quickly. As a result, according to Reaction (5), the released OH^- in the solution will increase the pH value of the solution rapidly to a relatively high value. As the pH increases, Reaction (6) by which $Mg(OH)_2$ is formed may be promoted. Therefore, the pH value will be decreased.

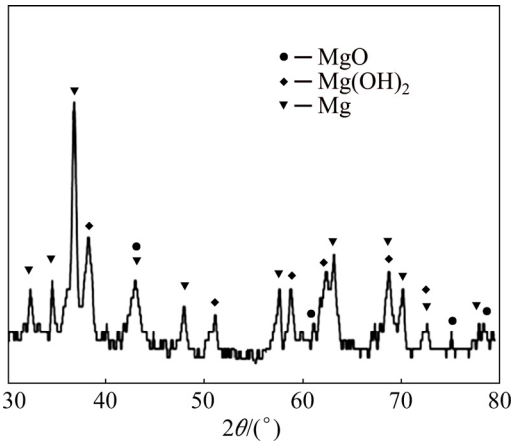

Fig. 6 XRD pattern of Mg−6Al−1Zn−1Si alloy immersed for 4 d

The creation of these protective layers can reduce the corrosion rate and prevent higher increase in the pH value. Such a protective layer has caused the pH value to approximately remain constant in 2-, 3- and 4-day immersion test (see Fig. 7) [31,32].

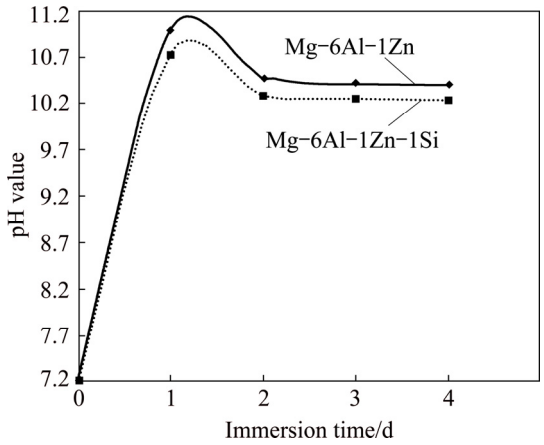

Fig. 7 Variation of pH value in Ringer solution with immersion time

3.3 Cytotoxicity of Mg-based alloys

Figure 8 shows the cell viability cultured in Mg−6Al−1Zn and Mg−6Al−1Zn−1Si alloy extraction medium for 1, 2, 3 and 4 d. The results indicate that Mg−6Al−1Zn−1Si system extracts show better cell viability compared to Mg−6Al−1Zn. By increasing the MTT test time, a slight increase in cell viability in both samples is also notable. Compared to Mg−6Al−1Zn−1Si alloy, the higher corrosion rate of Mg−6Al−1Zn system has resulted in higher change of pH value of the extraction medium, thus reduced the cell viability of Saos-2 cells (see Fig. 8). Mg−6Al−1Zn alloy has indicated a current density of 43% and its corrosion rate can be calculated to be 2.44 mm/year compared to 58% and 2.2 mm/year, respectively, for the Mg−6Al−1Zn−1Si system.

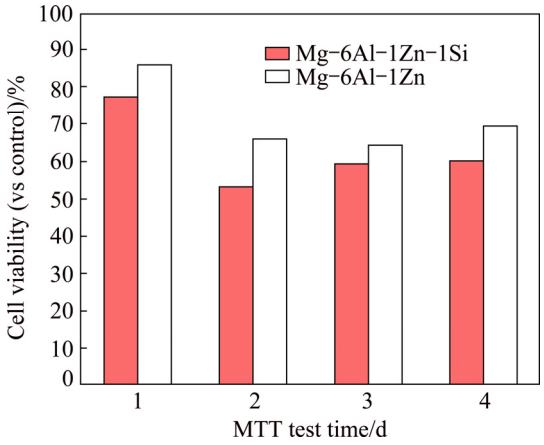

Fig. 8 Cell viability of alloys expressed as percentage of cell viability in control after 1, 2, 3 and 4 d

ZHANG et al [35] has demonstrated that high pH value of the extraction can cause serious hemolysis when the pH value is higher than 10.2.

Additionally, corrosion rate of Mg depends on solution loading capacity of Mg ions as well as pH [36], and metal ions released in MTT test can cause the cytotoxicity [6,11]. The Mg concentrations of Mg−6Al−1Zn and Mg−6Al−1Zn−1Si alloy extracts are shown in Fig. 9. In this study, the Mg ion concentration has gradually been increased during MTT test; in contrast, cell viability is improved after 2, 3 and 4 d. Furthermore, the Zn content in Mg alloy is less than 6%. ZHANG et al [11] has reported that the addition of 1.5% Zn to Mg−0.6Si alloy has not reflexed cytotoxicity. Overall, the higher pH value of Mg−6Al−1Zn composite extract may be the main reason of the higher toxicity of Saos-2 cells.

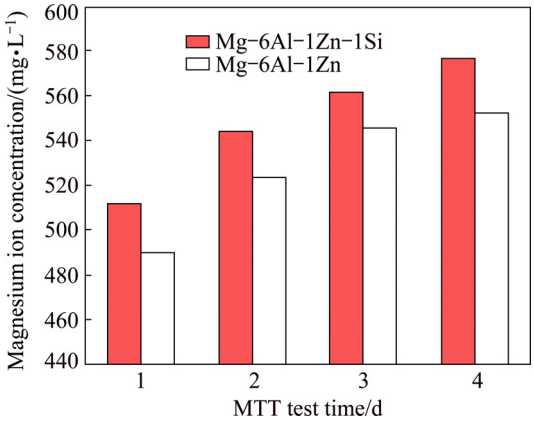

Fig. 9 Magnesium ion concentrations of alloy extracts after 1, 2, 3 and 4 d

4 Conclusions

1) Although grain sizes of both material systems increased after hot pressing, Si-containing system displayed a smaller grain size, i.e., 63 nm compared to 71 nm in Mg−6Al−1Zn system, after being exposed to 350 °C for 1 h.

2) The second-phase intermetallic particle Mg_2Si formed during hot pressing in Mg−6Al−1Zn−1Si system could influence not only the mechanical properties but also the bio-corrosion properties.

3) MTT test results have indicated that the higher pH value of Mg−6Al−1Zn alloy extract may be the main reason for the higher toxicity of Saos-2 cells compared to Mg−6Al−1Zn−1Si alloy extract.

Acknowledgements

The authors would like to thank Cellular and Molecular Biology Research Center in Babol University of Medical Sciences, especially Dr. Ebrahim Zabihi for their cooperation and assistance.

References

[1] KIRKLAND N T, BIRBILIS N, STAIGER M P. Assessing the corrosion of biodegradable magnesium implants: A critical review of current methodologies and their limitations [J]. Acta Biomaterial, 2012, 8(3): 925−936.

[2] HOU L, LI Z, PAN Y, DU L, LI X, ZHENG Y, LI L. In vitro and in vivo studies on biodegradable magnesium alloy [J]. Progress in Natural Science: Materials International, 2014, 24(5): 466−471.

[3] LI L, GAO J, WANG Y. Evaluation of cyto-toxicity and corrosion behavior of alkali-heat-treated magnesium in simulated body fluid [J]. Surface and Coatings Technology, 2004, 185(1): 92−98.

[4] CUI L, XU J, LU N, ZENG R C, ZOU Y H, LI S Q, ZHANG F. In vitro corrosion resistance and antibacterial properties of layer-by-layer assembled chitosan/poly-*L*-glutamic acid coating on AZ31 magnesium alloys [J]. Transactions of Nonferrous Metals Society of China, 2017, 27(5): 1081−1086.

[5] LI N, ZHENG Y. Novel magnesium alloys developed for biomedical application: A review [J]. Journal of Materials Science & Technology, 2013, 29(6): 489−502.

[6] ERDMANN N, ANGRISANI N, REIFENRATH J, LUCAS A, THOREY F, BORMANN D, LINDENBERG A M. Biomechanical testing and degradation analysis of MgCa0.8 alloy screws: A comparative in vivo study in rabbits [J]. Acta Biomaterialia, 2011, 7(3): 1421−1428.

[7] GU X, ZHENG Y, CHENG Y, ZHONG S, XI T. In vitro corrosion and biocompatibility of binary magnesium alloys [J]. Biomaterials, 2009, 30(4): 484−498.

[8] SONG G, ATRENS A, DARGUSCH A. Influence of microstructure on the corrosion of diecast AZ91D [J]. Corrosion Science, 1998, 41(2): 249−273.

[9] WITTE F, KAESE V, HAFERKAMP H, SWITZER E, MAEYER-LINDENBERG A, WIRTH C J, WINDHAGEN H. In vivo corrosion of four magnesium alloys and the associated bone response [J]. Biomaterials, 2005, 26(17): 3557−3563.

[10] SONG G, ATRENS A. Understanding magnesium corrosion—A framework for improved alloy performance [J]. Advanced Engineering Materials, 2003, 5(12): 837−858.

[11] ZHANG E, HE W, DU H, YANG K. Microstructure, mechanical properties and corrosion properties of Mg−Zn−Y alloys with low Zn content [J]. Materials Science and Engineering A, 2008, 488(1): 102−111.

[12] ZHANG E, YANG L, XU J, CHEN H. Microstructure, mechanical properties and bio-corrosion properties of Mg−Si(−Ca, Zn) alloy for biomedical application [J]. Acta Biomaterialia, 2010, 6(5): 1756−1762.

[13] YIN D, ZHANG E, ZENG S. Effect of Zn on mechanical property and corrosion property of extruded Mg−Zn−Mn alloy [J]. Transactions of Nonferrous Metals Society of China, 2008, 18(4): 763−768.

[14] ZHANG D F, SHI G L, DAI Q W, WEI Y, DUAN H L. Microstructures and mechanical properties of high strength Mg−Zn−Mn alloy [J]. Transactions of Nonferrous Metals Society of China, 2008, 18(1): 59−63.

[15] ZHANG E, YIN D, XU L, YANG L, YANG K. Microstructure, mechanical and corrosion properties and biocompatibility of Mg−Zn−Mn alloys for biomedical application [J]. Materials Science and Engineering C, 2009, 29(3): 987−993.

[16] HE W, ZHANG E, YANG K. Effect of Y on the bio-corrosion behavior of extruded Mg−Zn−Mn alloy in Hank solution [J]. Materials Science and Engineering C, 2010, 30(1): 167−174.

[17] SRINIVASAN A, NINGSHEN S, MUDALI U K, PILLAI U T S, PAI B C. Influence of Si and Sb additions on the corrosion behavior of AZ91 magnesium alloy [J]. Intermetallics, 2007, 15(12): 1511−1517.

[18] ZHENG Y F, GU X N, XI Y L, CHAI D L. In vitro degradation and cytotoxicity of Mg/Ca composites produced by powder metallurgy [J]. Acta Biomaterialia, 2010, 6(5): 1783−1791.

[19] SUN B, LI S, IMAI H, UMEDA J, KONDOH K. Synthesis kinetics of Mg_2Si and solid-state formation of Mg−Mg_2Si composite [J]. Powder Technology, 2012, 217: 157−162.

[20] MCCARTY M F. Reported anti atherosclerotic activity of silicon may reflect increased endothelial synthesis of heparan sulfate proteoglycans [J]. Medical Hypotheses, 1997, 49(2): 175−176.

[21] METAYER J, BING Y E, WEI G U O, WANG Q, HAO Z, MOLLET F. Microstructure and mechanical properties of Mg−Si alloys processed by cyclic closed-die forging [J]. Transactions of Nonferrous Metals Society of China, 2014, 24(1): 66−75.

[22] WANG L, QIN X Y. The effect of mechanical milling on the formation of nanocrystalline Mg_2Si through solid-state reaction [J]. Scripta Materialia, 2003, 49(3): 243−248.

[23] XIONG W, QIN X Y, KONG M G, LI C. Synthesis and properties of bulk nanocrystalline Mg_2Si through ball-milling and reactive hot-pressing [J]. Transactions of Nonferrous Metals Society of China, 2006, 16(5): 987−991.

[24] WILLIAMSON G K, HALL W H. X-ray line broadening from filed aluminium and wolfram [J]. Acta Metallurgica,1953, 1(1): 22−31.

[25] Standard G31−72. Practice for laboratory immersion corrosion testing of metals [S]. ASTM Stand. Philadelphia: Am Soc Test Mater, 2004.

[26] RAZAVI M, FATHI M H, MERATIAN M. Microstructure, mechanical properties and bio-corrosion evaluation of biodegradable AZ91-FA nanocomposites for biomedical applications [J]. Materials Science and Engineering A, 2010, 527(26): 6938−6944.

[27] MOTAVALLI A, RAJABI M. Catalytic effect of melt-spun Ni_3FeMn alloy on hydrogen desorption properties of nanocrystalline MgH_2 synthesized by mechanical alloying [J]. International Journal of Hydrogen Energy, 2014, 39(30): 17047−17053.

[28] RIAHI S, RAJABI M, RABIEE S M. Characterization of porous Ti-bioglass composite produced by mechanical milling and space holder sintering [J]. Rare Metals, 2015, 34(9): 638−644.

[29] ZENER C, SMITH C. Grains, phases and interfaces: Interpretation of microstructures [J]. Transactions Metallurgy Society of AIME, 1949, 175: 15−51.

[30] LUCAK P, TROJANOVA Z. Influence of grain size on ductility of magnesium alloys [J]. Materials Engineering, 2011, 18(2): 110−114.

[31] ZHAO C Y, PAN F S, PAN H C. Microstructure, mechanical and bio-corrosion properties of as-extruded Mg−Sn−Ca alloys [J]. Transactions of Nonferrous Metals Society of China, 2016, 26(6): 1574−1582.

[32] BEN-HAMU G, ELIEZER D, SHIN K S. The role of Mg_2Si on the corrosion behavior of wrought Mg−Zn−Mn alloy [J]. Intermetallics, 2008, 16(7): 860−867.

[33] LI Y, LU F, LI H, ZHU W, PAN H, TAN G, LAO Y, NING C, NI G. Corrosion mechanism of micro-arc oxidation treated biocompatible AZ31 magnesium alloy in simulated body fluid [J]. Progress in Natural Science: Materials International, 2014, 24(5): 516−522.

[34] ALTUN H, SEN S. Studies on the influence of chloride ion concentration and pH on the corrosion and electrochemical behaviour of AZ63 magnesium alloy [J]. Materials & Design, 2004, 25(7): 637−643.

[35] ZHANG S, LI J, SONG Y, ZHAO C, ZHANG X, XIE C, ZHANG Y, TAO H, HE Y, JIANG Y, BIAN Y. In vitro degradation, hemolysis and MC3T3-E1 cell adhesion of biodegradable Mg−Zn alloy [J]. Materials Science and Engineering C, 2009, 29(6): 1907−1912.

[36] HARRISON R, MARADZE D, LYONS S, ZHENG Y, LIU Y. Corrosion of magnesium and magnesium−calcium alloy in biologically-simulated environment [J]. Progress in Natural Science: Materials International, 2014, 24(5): 539−546.

添加 Si 对 Mg−6Al−1Zn 合金显微组织、力学性能、生物腐蚀和细胞毒性的影响

M. AMIRNEJAD, M. RAJABI, A. MOTAVALLI

Department of Materials Science and Engineering, Faculty of Mechanical Engineering,
Babol Noshirvani University of Technology, P. O. Box 47148-71167, Shariati Street, Babol, Iran

摘　要：用机械合金化和热压法制备可降解的 Mg−6Al−4Zn 金属植入体。通过 X 射线衍射分析、透射电镜、压缩试验、浸泡试验、电化学测试和 MTT 比色法研究添加 1% Si(质量分数)对 Mg−6Al−1Zn 合金显微组织、力学性能、生物腐蚀行为和细胞毒性的影响。结果显示，添加 1% Si 后，Mg−6Al−1Zn 中形成了细小的多边形 Mg_2Si 相，材料的抗压强度、伸长率和耐腐蚀性能提高，且骨肉瘤(Saos-2)细胞的细胞活性提高。根据 MTT 测试结果，释放出的镁离子没有细胞毒性。因此，添加 1% Si 提高了 Mg−6Al−4Zn 作为可降解植入体的综合性能。

关键词：镁基合金；机械合金化；力学性能；腐蚀速率；细胞活性

(Edited by Wei-ping CHEN)